ACS APPLIED MATERIALS & INTERFACES

www.acsami.org

Research Article

Enhanced Emission of Zinc Nitride Colloidal Nanoparticles with Organic Dyes for Optical Sensors and Imaging Application

Soundharraj Prabha, Dhinasekaran Durgalakshmi,* Karthikeyan Subramani, Prakasarao Aruna, and Singaravelu Ganesan

Cite This: *ACS Appl. Mater. Interfaces* 2020, 12, 19245−19257

Read Online

ACCESS | Metrics & More | Article Recommendations | Supporting Information

ABSTRACT: Herein, we have reported on the efficiency of inorganic Zn_3N_2 nanoparticles for labeling plant cells and animal cells toward imaging applications with negligible toxicity. We have synthesized zinc nitride (Zn_3N_2) colloidal nanoparticles with an average size of 25 nm at room temperature. The optical band gap of the prepared Zn_3N_2 nanoparticles is 2.8 eV and gives a visible range emission at 415 nm. With the addition of Zn_3N_2 colloids to organic dyes such as protoporphyrin, flavin adenine dinucleotide, fluorescein, and neutral red, the emission intensity of the organic dyes enhanced from 3 to 20 times. The molecular simulation and lifetime studies evidence the possibility of energy transfer from zinc nitride to organic dyes. The enhancement of dye intensity in the presence of Zn_3N_2 enhanced the vicinity of the cellular environment during confocal imaging of plant cells and animal cells. The detailed results suggested Zn_3N_2 for bioimaging and biosensor applications.

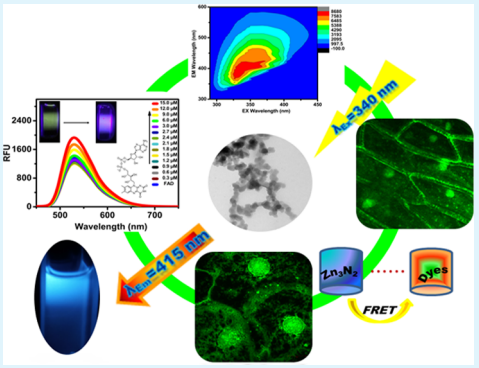

KEYWORDS: *zinc, docking, spectroscopy, sensor, imaging*

INTRODUCTION

Imaging is a significant platform for the diagnosis of diseases at an early stage, and it helps to make therapeutic plans. In particular, cellular level diagnosis is considered as a challenge in the biomedical research. There are various modes of techniques used for bioimaging in clinics and diagnostic centers, such as computed tomography, magnetic resonance imaging (MRI), and positron emission tomography. These topographic imaging techniques have a limitation of real-time imaging for therapy. However, the optical bioimaging is considered as superior to other conventional imaging techniques because of the sophistication of real-time live imaging.[1,2] Over three decades, fluorescent nanomaterials are used for recording the information related to biomolecules using various optical equipment, and it also shows the possibility of interacting with ligands, with its application extending to theranostics.[3]

The recent progresses of bioimaging include fluorescence imaging microscopy and fluorescence resonance energy transfer (FRET).[4] There are several techniques related to bioimaging such as in vivo cell tracking, labeling, and imaging. Fluorescent labeling combined with staining is widely used in the biomedicine field because of its sensitivity. The fluorescent probe allows sensitive detection of biological molecules with high resolution. Fluorescent imaging is possible from (i) intrinsically fluorescent reduced nicotinamide adenine dinucleotide (NADH), tissues, and chlorophyll and (ii) induced fluorescence of cells and samples with the addition of dye staining.[5] In general, fluorescence imaging can be attained through the measurements of intensity (quenching or enhancement), lifetime ,and resonance energy transfer.[6] Förster resonance energy transfer (FRET) is a powerful technique used to study nano-bio combination for bioimaging applications.[7] FRET based on organic dyes can be achieved by simple preparation methods at low cost. However, these dyes have short lifetime and low chemical stability, making it challengeable for the production of FRET in organic dyes.

FRET in the presence of nanoparticles provides spatial and kinetic information about the interaction between the fluorescent nanoparticle and protein in the cell environment.[8] Inorganic nanoparticles such as gold and silver gives fluorescence signals enhanced by the surface plasmon with greater sensitivity for imaging and biosensing applications.[9] The maximum fluorescence enhancement depends on the decay rate (nonradiative and radiative decay rate) and quantum efficiency. In order to achieve FRET, the distance between the fluorophore and the nanoparticles needs precise selection. A very less distance may cause fluorescence quenching and a long distance may not cause fluorescence

Received: November 28, 2019
Accepted: April 3, 2020
Published: April 3, 2020

https://dx.doi.org/10.1021/acsami.9b21585
ACS Appl. Mater. Interfaces 2020, 12, 19245−19257

enhancement.[10] Thus, FRET is a more sensitive distance-dependent fluorescence signal for monitoring molecular interactions in vitro and in vivo.

Even though organic molecules possess photochemical instability and nonoptimum spectroscopic properties, it is often used as a fluorescent label for in vivo imaging. These organic molecules are also available as commercial sources for versatile fluorescence applications.[11] Nevertheless, they hardly interact with the cellular organelle and affect the optical properties, and low tissue absorbance exhibits photothermal effects. In most of the cases, organic dyes were used as probes because of their high quantum efficiency. However, optically stable sensitive dyes are in need for real-time analysis and detection of biomolecules. The major drawback in achieving organic stable dyes is photobleaching of the dyes at powerful excitation energies.[12] Earlier work shows that nano structures combined with fluorescence organic dyes provide enhanced signals even in the presence of very small tumor species.[13] Functionalization with inorganic nanomaterials enables imaging with reduced toxicity and enhances the brightness with low background noises. Compared to widely used organic dyes, semiconductor quantum dots and nanoparticles are attractive in imaging due to optical property, stability, brightness, lesser photobleaching, and high detection limit.[13−16] The inorganic nanoparticles include luminescent silica nanoparticles,[17,18] carbon dots,[16] nanotubes, nanoclusters, nanodiamonds, and metal oxides.[19] Colloidal quantum dots such as CdS,[20] CdSe,[21] CdTe, PbS,[22] PbSe,[23] and HgTe[24] have potential cytotoxicity during in vitro and in vivo despite efficient photo emission.[25] Hence, recent research is much focused on developing inorganic nanomaterials, which act as sensitive probes with low toxicity and high stability. In addition to the aforementioned inorganic nanomaterials, aggregated induced emission fluorescent materials, conjugated with biological components such as peptides, carbohydrates, and nucleic acids are used as probes in imaging application.[1] The metal nanoclusters such as gold, silver, copper, and platinum are also in use for cellular imaging and drug delivery application.[3] Recently, near infrared fluorescence imaging was considered as important in tissue scattering and auto fluorescence, which can be applied for in vivo imaging because of the high signal to background ratio. However, the toxicity of Nd^{3+}, Er^{3+}, and Yb^{3+}-doped lanthanum nanoclusters used in imaging application needs to be explored in future.[2]

Among all biocompatible materials, zinc is the necessary nutrient for human life, and most of the body functions are connected with zinc-containing enzymes. It is considered as the second most transition metal ion in living organisms, and it plays an essential role in maintaining human health diseases.[26,27] Zinc is classified into three functional categories: (i) structural function, (ii) catalyst, and (iii) regulatory function.[28] The unique properties of this material are biocompatibility, stability, and ability to use in biomedical applications.[15] Zinc nitride (Zn_3N_2) has potential optoelectronic and photovoltaic electronic properties, with good chemical stability and also suggested for a cost-effective solar material.[29] It belongs to the semiconductor II−IV group with high carrier concentration and electron mobility. The first-principles calculation shows that Zn_3N_2 has the highest bond strength [2.562 eV for Zn−N(2) and 1.764 eV for Zn−N(1)] and lowest electron effective mass [$(0.08-0.03)m_o$].[29] In 1940, Juza et al. synthesized Zn_3N_2 powder for the first time, and it remained as an unresearched material over 50 years. Later in 1993, Kuriyama et al.[30] prepared a zinc nitride film using the direct reaction between zinc and ammonia and evaporated onto the quartz substrate with the band gap of 2.2−2.4 eV.[31] Based on the preparation technique, the bandgap values varied from 1.0 to 3.3 eV.[32] As this material is highly suggested for optoelectronic devices, literature studies reported on preparing this material as thin films by physical methods such as RF sputtering[33,34] and pulsed laser deposition.[35] The band gap of Zn_3N_2 is still debatable in the concept of narrow or wide band gap and direct or indirect bandgap, where it needs lot of theoretical understanding. Very few literature studies have reported on the optical properties of Zn_3N_2,[36,37] focusing further toward optoelectronic applications. The biological applications of Zn_3N_2 are not yet examined similar to other inorganic nanoparticles such as gold, silver, CdS, CdSe and so forth.

In the present work, a Zn_3N_2 colloid was prepared by chemical methods toward bioimaging application. With the advent of synthesis by chemical methods,[37] we can tune the structural and optical properties of the nanoparticles. Further, the interaction of Zn_3N_2 with organic dyes and cellular uptake were studied in detail. The improved imaging performance was verified on both plant cells and human fibroblast cells using confocal microscopy.

EXPERIMENTAL SECTION

Chemicals and Reagents. In order to prepare Zn_3N_2, chemicals such as zinc acetate dihydrate extra pure ($Zn(CH_3CO_2)\cdot 2H_2O$), ammonia solution (NH_3, 30%), ethanol (99.9%), and oleic acid pure ($C_{18}H_{34}O_2$, 65−88%) were purchased in analytical grade from Sigma-Aldrich and Sisco Research Laboratories Pvt. Ltd. (SRL) and used without further purification.

In brief, zinc acetate dihydrate was added with ammonia solution in the presence of oleic acid, which acts as a capping agent. Zinc acetate dihydrate (1 mmol, 100 μL) was added to the mixture of 0.5 mL of oleic acid and 15 mL of ethanol at room temperature and stirred for 5 min. In order to undergo the nitridation process, 2.5 mL of ammonia solution was injected to the zinc solution. The end colloid was stirred for 1 h, which results in the homogenous transparent Zn_3N_2 colloidal formation. The colloidal solution is stored in the ambient temperature for further process.

Characterization. The functional groups were analyzed from FTIR spectra using Fourier transform infrared spectroscopy (FTIR) (JASCO FT/IR-6600). The bonding configuration was determined using Raman spectrometer LabRam HR 800 (HORIBA JobinYvon, France) with an air-cooled intracavity laser point source (model DL 785-100) of 488 nm argon as an excitation source. The absorption and the emission spectrum were obtained using a microplate reader (Spectramax M5). The luminescence color was captured from the Fluoromax-2 (HORIBA JobinYvon-SPEX, Edison, New Jersey, USA) using fibre optic probe. Transmission electron microscopy, TEM (Tecnai T12 G2 sprit-cryo TEM), was utilized to obtain the internal morphology of the samples. The particle size distribution was studied using dynamic light scattering (ZEN3600). Aqualog ((HORIBA Scientific) was employed to study the excitation emission matrix. Fluorescence lifetime was measured using the time-correlated single photon counting measurements (TCSPC) in Fluorolog (Fluorolog HORIBA JobinYvon). The images of plant cell (onion peel) and 3T3 cells were imaged with a confocal laser scanning microscope (ZEISS LSM 880) using 405, 458, 488, and 561 nm laser excitation source for porphyrin, flavin adenine dinucleotide (FAD), fluorescein, and neutral red, respectively.

Docking Studies. The compound (protoporphyrin, FAD, fluorescein, and neutral red) structure was drawn using chem. Draw pro 12 software and the zinc nitride structure were obtained from crystallography information file using Mercury 3.9 software for further docking study.[38,39] The converted structure compound was energy

https://dx.doi.org/10.1021/acsami.9b21585
ACS Appl. Mater. Interfaces 2020, 12, 19245−19257

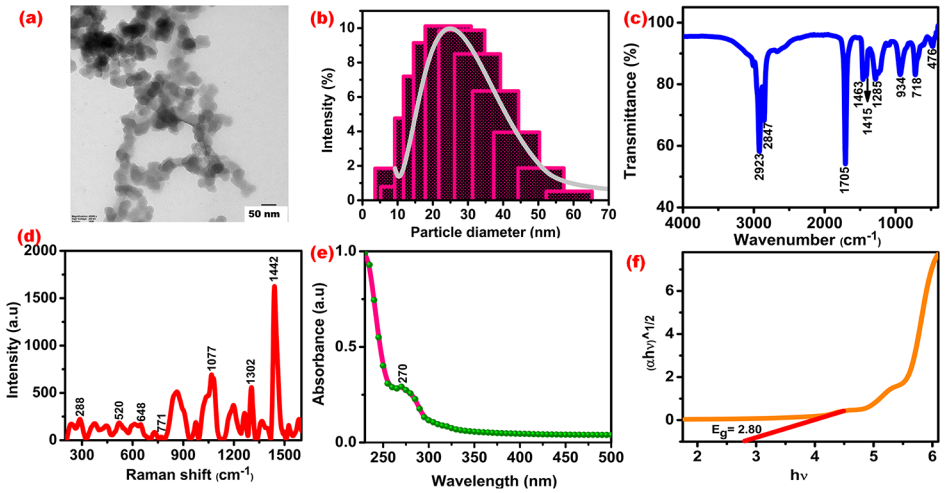

Figure 1. Structural characterization of Zn_3N_2. (a) TEM image of hexagonal shaped particles with an average particle size around 25 nm, (b) DLS particle size distribution shows an average particle size around 24.3 nm, (c) FTIR spectrum, (d) Raman spectrum confirms the presence of Zn and N, (e) UV−vis spectrum shows the maximum absorption wavelength at 270 nm, and (f) Tauc plot from UV−vis spectrum gives an optical bandgap of 2.80 eV.

minimized and optimized based on steepest descent and followed by conjugate gradient algorithm using dock prep application. The rigid roots were automatically set for small molecules, and all possible torsion and rotatable bonds are mentioned as active. The default grid parameter was used to make a grid box on the active site of the compound with a size of 125 Å × 125 Å × 125 Å and 0.3125 Å grids spacing using AutoGrid program. Using Lamarckian genetic algorithm with AutoDock 4.2 tool,[40−42] the flexible docking was performed between compound and Zn_3N_2 crystal structure. The obtained output files were analyzed using PyMOL software.

Cell Culture. 3T3 fibroblast cell lines were procured from Tamil Nadu Veterinary and Animal Sciences University (TANUVAS), Chennai. The cell lines were seeded in the T25 flask (75 cm^2) in Dulbecco's modified Eagle's medium (DMEM) along with fetal bovine serum (FBS) and penicillin/streptomycin. The cells were cultured under standard conditions at 37 °C in 5% CO_2 incubator. The medium was replaced every 48 h, and the confluence of cells were monitored through a microscope. When the confluent level reached above 60%, the cells were washed using phosphate buffer saline (PBS) and separated with the help of trypsin and subculture into a newer flask.

Bioimaging Studies. For bioimaging studies, 3T3 fibroblast cell lines were seeded on the coverslips in 8 well plates. The cells were cultured in DMEM containing FBS and antibody for 24 h at 37 °C in 5% CO_2 incubator. After 24 h, the monolayer cell lines were rinsed with PBS and incubated with 10 μL of chosen organic dyes and organic dyes@Zn_3N_2 at 37 °C for 20 min; then the fluorescence image was studied using the confocal laser scanning microscope.

Cytotoxicity by MTT Assay Method. For MTT assay, 3T3 fibroblast cell lines were seeded in 96 well plates at a density of 1 × 10^4 cell per well, and the cells were incubated at 37 °C in a CO_2 incubator for 24 h. After that, the cells were treated with zinc nitride nanocolloids of various concentrations from 0.3 to 1.5 μM in triplicate and incubated for 24 h. In order to remove the unattached cells in the well plate, the cells were washed using PBS. After which, 10 μL of 2 mg/2 mL of 3-(4,5-dimethylthiazol-2-yl)-2,5-diphenyltetrazolium bromide (MTT dye) solution was added to each well, and the untreated cells were considered as a control reference. Later, it was incubated for 4 h at 37 °C in incubator under 5% CO_2. The cell toxicity was determined through measuring the optical density at 540 nm in a SpectraMax-5 microplate reader, and the % of cytotoxicity is calculated.

RESULTS AND DISCUSSION

The shape and size of Zn_3N_2 nanoparticles were observed using TEM (Figure 1a). The morphology shows hexagonal shaped particles with an average particle size around 25 nm. The particles under different magnification observed under TEM are shown in Figure S2. The elemental analysis and crystal structure confirmed using energy-dispersive X-ray spectrometry and X-ray diffraction (XRD) are shown in Figures S3 and S1, respectively. The XRD analysis Zn_3N_2 colloid coated on glass substrates confirms the formation of a Zn_3N_2 crystal structure from the major peaks matched with JCPDS 35-0762 (Figure S1). The result from the particle size analyzer also confirms the average particle size around 24.3 nm (Figure 1b). The presence of functional groups in the colloidal solution can be observed using FTIR and Raman spectroscopy. In the FTIR spectrum (Figure 1c), the peaks observed at 2923 and 2847 cm^{-1} are due to the CH_2 asymmetric stretching and CH_2 symmetric stretching, respectively. Peaks at 1705, 1463, 1285, 934$^-$, and 718 cm^{-1} indicated the presence of C═O stretching, in plane O−H bond, C−O stretching, out of plane O−H stretching, and CH_2 rocking functionalities, respectively. The presence of zinc and nitrogen bonding with zinc is confirmed from the respective peaks at 476 and 1415 cm^{-1}.[43]

Figure 1d plots the Raman spectrum for Zn_3N_2 nanoparticles, where we can observe peaks at 1442 and 1302 cm^{-1} corresponding to the CH_2 bond, and the peak at 1077 cm^{-1} is due to C−C vibrations. The local vibrational modes of N are observed at 288, 648$^-$, and 771 cm^{-1}.[44−46] The peak at 520 cm^{-1} is attributed to Si−O vibration arises from the glass substrate.[47] The UV−vis spectrum of Zn_3N_2 (Figure 1e) depicts the absorption wavelength at 270 nm. The optical band gap (E_g) of Zn_3N_2 was calculated from the Tauc's relation: $(\alpha h\nu) = (h\nu - E_g)^n$, where α is the absorption coefficient and $h\nu$ is the photon energy. The value of E_g calculated from the intercept of the linear fitted lines in the plots of $h\nu$ versus $(\alpha h\nu)^{1/2}$ and found to be 2.80 eV (Figure 1f). The band gap can be increased with respect to the quantity of oxygen present in Zn_3N_2.[48] Many researchers analyzed on oxygen-induced defects in zinc nitride, where oxygen is substituted in the nitrogen lattice position.[49] Even though the presence of Zn−O

https://dx.doi.org/10.1021/acsami.9b21585
ACS Appl. Mater. Interfaces 2020, 12, 19245−19257

bond is confirmed from FTIR, the lesser band gap value compared to earlier literature studies shows that the oxygen-induced defect is lesser in the present method of preparing Zn_3N_2 nanoparticles.

The excitation−emission matrix was recorded from 240 to 700 nm (Figure 2a). The highest fluorescence intensity was

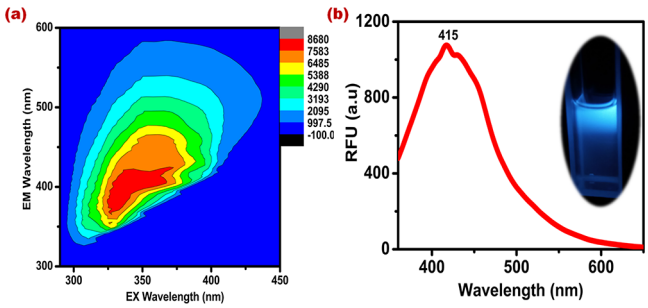

Figure 2. (a) Excitation−emission matrix of Zn_3N_2, highest fluorescence intensity was observed at 415 nm, with an excitation wavelength of 340 nm and (b) fluorescence blue emission of Zn_3N_2 for 340 nm excitation.

observed at 415 nm, with an excitation wavelength of 340 nm. Hence, 340 nm was selected as the optimum excitation wavelength of Zn_3N_2 for emission of 2D spectrum (Figure 2b). For this wavelength, the emission at various concentrations of nanoparticles was obtained, and the quantum efficiency was calculated as 59%. In order to prove that the emission is merely due to the formation of Zn_3N_2, we obtained the emission spectra of all the chemical agents used in the synthesis of the nanoparticles (Figure S4). The stability of the Zn_3N_2 colloidal nanoparticle was analyzed from its emission intensity using photoluminescence spectroscopy, and it shows above 80% stability even after 60 days (Figure S5).

Interaction with Organic Dyes. Metallic nanoparticles with the dye molecules and their influence on the optical properties are an exciting research field in nanophotonics. The outcome of the research is quenching or enhancement of fluorescence properties of the dye molecule. It is assigned to the energy transfer between donor and acceptor molecules. In this work, we studied the interaction of Zn_3N_2 with different fluorescent dyes such as protoporphyrin IX, FAD, fluorescein, and neutral red. Protoporphyrin is a photosensitizing drug, which has attracted great attention in the field of photodynamic and photothermal therapy for treating skin tumors. It can conjugate with the aromatic molecules and exhibits attractive spectroscopic properties. Naturally, it is produced in the heme biosynthesis of biological systems.[50−52] Our body also has diverse molecules with auto fluorescence natives such as NADH, FAD, porphyrin, collagen, and tryptophan. By quantifying the properties of these dyes, certain stages of diseases can be diagnosed and treatment can be provided accordingly.[53] Furthermore, the FAD and NADH are also important to study the oxidation−reduction state of the cells.[54,55] Fluorescein dye and neutral red are used as an organic fluorescent dye in cell labeling and cell tracking. Neutral red belonging to the quinone imine class of dyes is a lysosomal probe and biological pH indicator. It is utilized in the optoelectronic field.[56] To overcome some of the limitations of organic dyes such as photobleaching and quenching, the optical properties of synthesized Zn_3N_2 nanoparticles integrated with aforementioned dye molecules were analyzed in detail.

The UV−visible absorption spectra studies were carried out to all the chosen dyes and dyes@Zn_3N_2 [1:6 μL] solutions individually in the range of 200−700 nm (Figure 3a,b).

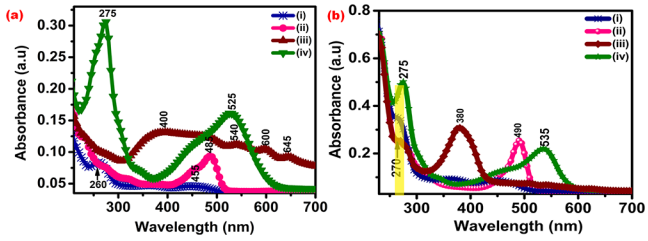

Figure 3. UV−vis spectrum of (a) dye alone, (i) FAD, (ii) fluorescein, (iii) porphyrin, (iv) neutral red, and (b) dye with nanoparticle (i) FAD@Zn_3N_2, (ii) fluorescein@Zn_3N_2, (iii) porphyrin@Zn_3N_2, and (iv) neutral red @Zn_3N_2.

Porphyrin has an absorption maximum in the soret band at 400 nm and in the Q-band at 540, 600, and 645 nm.[57] This revealed that it has a broad absorption window enabled to excite with multiple light sources. Porphyrin@Zn_3N_2 shows absorption at 380 nm; there occurs a hypsochromic effect after the addition of Zn_3N_2. The FAD dye exhibits a strong absorption peak at 260 and 445 nm attributed to $\pi-\pi^*$ transition in isoalloxazine rings,[54] and FAD@Zn_3N_2 have absorption at 445 and 360 nm. Fluorescein and fluorescein@Zn_3N_2 have absorption at 485 and 490 nm, with the shift of 5 nm. Neutral red and neutral red@Zn_3N_2 also possesses absorption at 525 and 535 nm with the shift of 10 nm. Other than porphyrin, rest of the dyes shows a bathochromic effect in the maximum absorption position, which depicts that Zn_3N_2 has positive influence on interaction with the organic dyes. In Figure 3b, the absorption of Zn_3N_2 is highlighted for confirming the presence of nanoparticles conjugated with dyes.

The binding affinity of the dyes with colloidal nanoparticles was estimated using UV−vis spectroscopy. The absorption spectra for the addition of Zn_3N_2 to the fixed concentration of dye molecules were collected, and the optical density gives the information about the binding affinity of the dye with nanoparticles (Figure S6).[58] The binding constant of dyes@Zn_3N_2 is calculated using Benesi−Hildebrand relation.[57] Figure 4 shows the double reciprocal graph between $1/(A_0 - A)$ versus 1/concentration for porphyrin@Zn_3N_2, FAD@Zn_3N_2, fluorescein@Zn_3N_2, and neutral red@Zn_3N_2 and depicts linear fit with the binding constant of 4.412×10^6, 4.393×10^6, $3.887 \times 10^{6\ -}$, and 2.519×10^6 M^{-1}, respectively. The binding constant proved that the dye molecules were well-tagged on the surface of the Zn_3N_2 colloidal nanoparticle.

To examine the emission spectrum for dyes@Zn_3N_2, the contour images recorded corresponds to the excitation emission matrix, and the excitation wavelength corresponding to the maximum emission was chosen for analysis of the 2D spectrum given in the inset of an individual spectrum. In Figure 5a, porphyrin@Zn_3N_2 holds a maximum emission at 538 nm and also possess many fluorophores in the matrix area of 400 nm. Thus, the 2D spectrum was obtained by excitation of both 400 and 538 nm (inset Figure 5a). The maximum emission of FAD@Zn_3N_2 (Figure 5b) occurs at 510 nm with an excitation of 480 nm and lesser fluorophore molecules present in the UV region (240−300 nm). The 2D spectrum

https://dx.doi.org/10.1021/acsami.9b21585
ACS Appl. Mater. Interfaces 2020, 12, 19245−19257

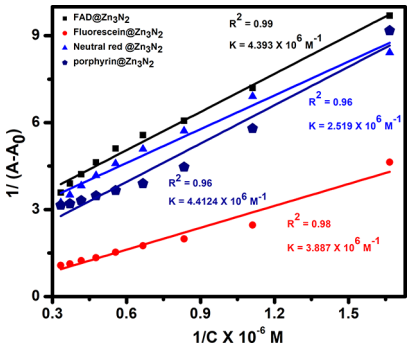

Figure 4. Double reciprocal plot between $1/A - A_0$ and 1/concentration (the data obtained from UV–vis spectra) to calculate binding between dyes and nanoparticles. The data plotted is obtained from UV–vis absorption spectral studies of dye absorption against various concentrations of zinc nitride colloidal nanoparticles (Figure S6).

emission FAD@Zn_3N_2 was observed at 480 nm excitation (inset Figure 5b). Similarly, in the case of fluorescein@Zn_3N_2, the CCD detector only records the emission in the UV region (240 nm). However, the same material was investigated by 2D emission spectrum, with an excitation of 490 nm emits green color with the wavelength of 520 nm (Figure 5c). The neutral red @Zn_3N_2 matrix shows the emission in two different regions at UV (240 nm) and visible red emission of 615 nm (Figure 5d). The 2D spectrum was obtained at the excitation of 535 nm, and the broad red emission spectrum is shown as the inset image.

Docking Study. In order to understand the type of interaction between Zn_3N_2 and organic dyes, computational simulation-based docking studies have been performed. In general, docking studies by computational methods play an important role for ligand target interaction studies. Molecular docking was carried out for the chosen organic dye and Zn_3N_2 toward understanding the energy transfer. It was considered to understand the reason for the resultant fluorescent enhancement from the ligand–target interaction. In this case, Zn_3N_2 acts as the ligand, and organic dyes as targets. Figure 6a shows the interaction of porphyrin with Zn_3N_2, where zinc molecules are attached with –NH and –N groups with an intermolecular distance of 2.8 and 2.6 Å, respectively. This distance prompted us to consider the possibility of the energy transfer process between nanoparticle and organic dye. For the molecules to perform as FRET, the intermolecular distance between the donor and the acceptor must be less than 10 Å. Thus, we performed docking for remaining samples such as FAD@Zn_3N_2 fluorescein@Zn_3N_2 and neutral red @Zn_3N_2.

In FAD with Zn_3N_2, we observed that more zinc molecules was bound to the site of OH and also with the –N group with an intermolecular distance 2.9–3.5 and 2.2–2.7 Å, respectively (Figure 6b). This result shows that the zinc nitride surface is hydrophilic in nature, and this is advantageous for utilizing this with bioconjugates of organic dyes and drugs, which opens the possibility of future therapy and diagnostic applications.

The docking results of fluorescein with Zn_3N_2 depict that the zinc molecules are bound to the site of the –COOH group with a distance of 2.5–3.4 Å (Figure 6c). In the case of neutral red, zinc was attached in the site of amine with an average distance of 2.5 Å (Figure 6d). Hence, the docking study revealed that Zn_3N_2 nanoparticles have a good interaction with the dye molecules, and this analysis was also considered as evidence on the energy transfer (FRET) toward optical enhancement.

Lifetime Study. With the evidence of the docking study with less intermolecular distance due the possibility of FRET, the lifetime of Zn_3N_2 conjugated with organic dyes was

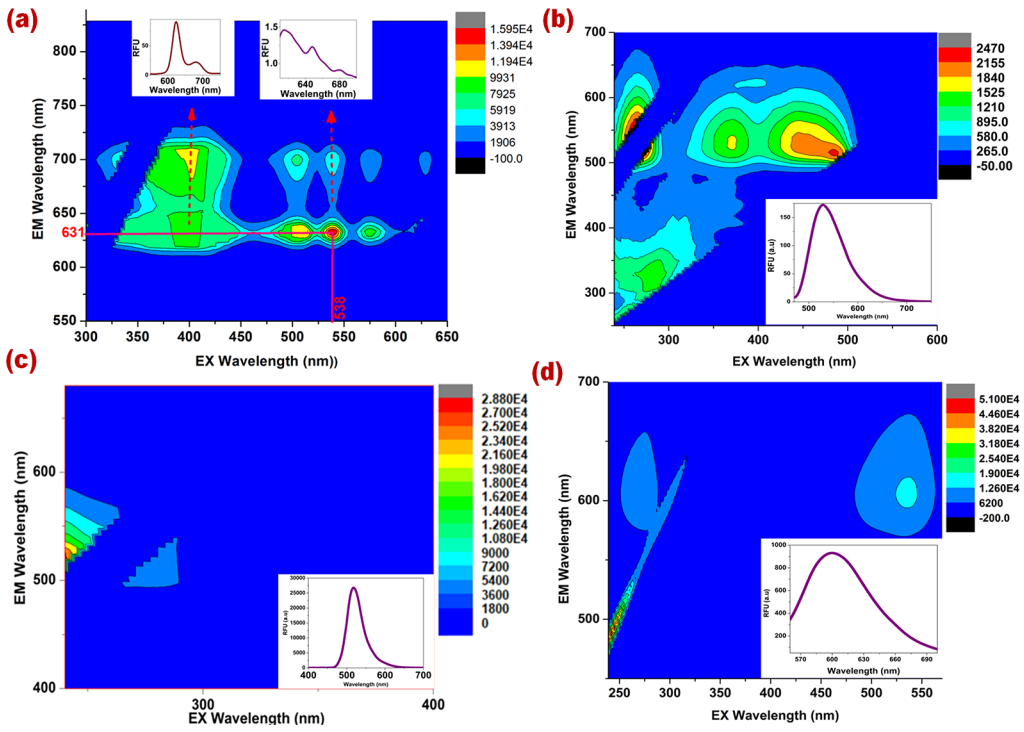

Figure 5. Excitation–emission matrix of (a) porphyrin@Zn_3N_2, (b) FAD@Zn_3N_2, (c) fluorescein@Zn_3N_2, and (d) neutral red@Zn_3N_2, and the inset shows the 2D spectrum using Spectromax.

https://dx.doi.org/10.1021/acsami.9b21585
ACS Appl. Mater. Interfaces 2020, 12, 19245–19257

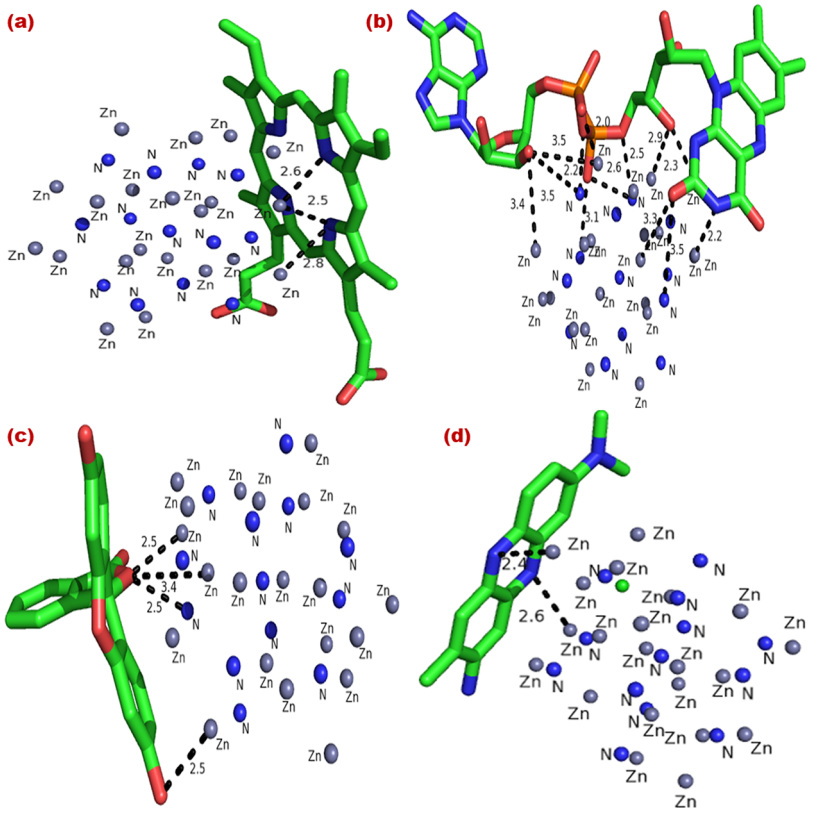

Figure 6. Docking study of (a) porphyrin@Zn_3N_2, (b) FAD@Zn_3N_2, (c) fluorescein@Zn_3N_2, and (d) neutral red @Zn_3N_2. It shows the intermolecular distance of 2.6−2.8, 2.9−3.5, and 2.5−3.4 and 2.5 Å, respectively.

Table 1. Fluorescence Lifetime Analysis

	slow component		fast component			
samples	τ_1 (ns)	B_1 (%)	τ_2 (ns)	B_2 (%)	χ^2	$\tau_0 = \frac{\sum \alpha_i \tau_0^2}{\sum \alpha_i \tau_i}$ (ns)
FAD	2.40	50.65	4.74	49.35	1.14	3.57
FAD@Zn_3N_2	2.56	57.59	4.86	42.41	1.25	3.71
fluorescein	2.08	17.11	4.31	82.89	1.10	3.20
fluorescein@Zn_3N_2	2.88	6.61	4.06	93.39	1.17	3.47
neutral red	0.56	62.92	0.99	37.08	1.27	0.78
neutral red@Zn_3N_2	1.69	93.87	3.56	6.13	1.23	2.63

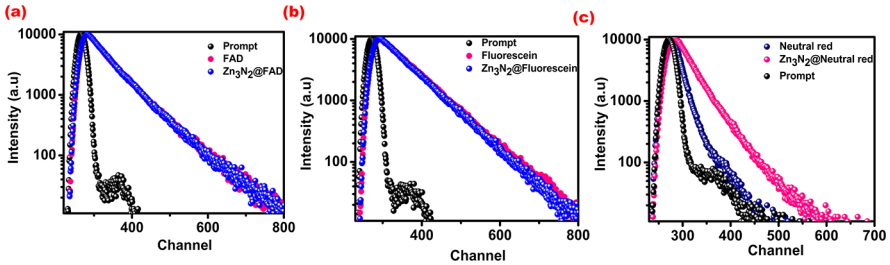

Figure 7. Lifetime measurements of organic dyes and organic dyes@Zn_3N_2, (a) FAD, (b) fluorescein, and (c) neutral red.

investigated. The time that a molecule persists in its excited state before reaching the ground state (lifetime) is very sensitive to the fluorophore. In the case of lung cancer, tissues of normal versus cancer can also be discriminated from the lifetime of FAD and NADH.[59] In our work, it is useful to investigate the lifetime of organic dyes and the organic dyes@ Zn_3N_2. The enhancement in the life time depends on the energy transfer from donor to acceptor molecule (FRET), and the average lifetime of the acceptor increases with the decrease of the donor molecule,[60] and the lifetime increases with the enhancement of fluorescent intensity.[61] The lifetime of dye and dye with Zn_3N_2 was measured using TCSPC, and the decay curves were examined using a nonlinear least square fitting method. Bi-exponential fitting was used to calculate decay cofactors such as A_1, A_2, τ_1, and τ_2, where A_1 and A_2 are the exponential coefficients (%), and τ_1 and τ_2 are the

https://dx.doi.org/10.1021/acsami.9b21585
ACS Appl. Mater. Interfaces 2020, 12, 19245−19257

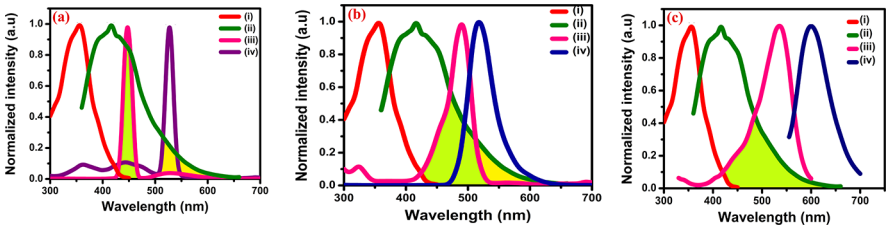

Figure 8. FRET in zinc nitride with dyes (a) FAD, (b) fluorescein, (c) neutral red (green colour—FRET, yellow—DSBT, and cyan—ASBT), (i) excitation of Zn_3N_2, (ii) emission of Zn_3N_2, (iii) excitation of dye, and (iv) emission of dyes.

corresponding lifetimes. The values of exponential coefficients and lifetimes with X^2 values are tabulated in Table 1.

The intensity related to number of molecules for a single exponential decay is expressed as

$$I(t) = I_0 \exp(-t/\tau) \quad (1)$$

where $I_o \rightarrow$ intensity at time $t = 0$. $\tau \rightarrow$ inverse of the total decay rate.

The fitted decay curve plotted in Figure 7a depicts that FAD@Zn_3N_2 has a greater lifetime compared to FAD alone, with the difference of 0.14 ns. Similarly, fluorescein@Zn_3N_2 has a long lifetime compared with dye alone (Figure 7b). In the decay curve (Figure 7c), there is a huge deviation (1.85 ns) for neutral red@Zn_3N_2. Hence, this TCSPC study confirms the energy transfer from donor of Zn_3N_2 to the acceptor of dyes and also leads to the study of fluorescent intensity enhancement.

Energy Transfer. From the docking study, the intermolecular distance may enable the energy transfer between nanoparticle and organic dye, and from the lifetime study, the quenching of donor lifetime with the increase of acceptor lifetime tends to move further toward the concept of FRET. This FRET technique provides more advantages compared with the conventional fluorescent labeling technique. The mechanism involves the nonradiative energy transfer from an excited donor to a ground state acceptor. The acceptor excitation is due to the emission of the donor; this leads to the quenching in the donor emission (Figure S7).[62−64] The FRET channel and background signal of donor spectral bleed through (DSBT) are highlighted in the Figure 8.[65,66] Previously, many standard fluorophores were developed for the donor/acceptor or both FRET system. In the present work, we have chosen organic dyes as acceptors and Zn_3N_2 as a donor (Figure S8).

The spectra of overlapping between emission spectra Zn_3N_2 and absorption spectra of dyes ensured the feasibility of the FRET. The emission spectra of organic dyes with the nanoparticle excited at a wavelength of 340 nm (λ_{ex} of Zn_3N_2 nanoparticle) are given in Figure S8, where, the spectrum gives both the emission of Zn_3N_2 and dye molecule. The emission intensity of Zn_3N_2 is quantitatively lesser compared to the dye, and this might be due to the enhanced emission intensity of the organic dye. In order to analysis the FRET process, the combination of excitation emission spectrum of Zn_3N_2 with the excitation emission spectrum of dyes such as FAD, fluorescein, and neutral red is depicted in Figure 8. In Figure 8a, the emission spectrum of Zn_3N_2 overlap with the excitation spectrum of FAD and the fluorescence intensity of the nanoparticle at 415 nm (λ_{ex} = 340 nm) was broadly interconnected with the FAD excitation and emission (λ_{em} = 530 nm; λ_{ex} = 445 nm). In this spectrum, nearly 90% of the energy is transferred from Zn_3N_2 to FAD. Even there is narrow overlapping of Zn_3N_2 emission with the excitation of FAD, and the broad energy transfer spectrum causes the fluorescence enhancement with the addition of Zn_3N_2. The spectral overlap region between the donor emission spectrum and acceptor absorption spectrum is illustrated in green. In addition, the spectral bleed through is also found in the FRET channel; thus the energy could have transferred directly from the donor inducing the transition in acceptor and the emission of acceptor bleed in donor absorption, which is in yellow. This will in turn affect the FRET efficiency (E). In Figure 8a, the tail region of excitation of the Zn_3N_2 tagged with the excitation and the emission spectrum of FAD. This broad overlapping may cause the admirable fluorescence enhancement.

In Figure 8b, the donor emission of Zn_3N_2 (415 nm) coupled with the acceptor excitation of fluorescein (λ_{ex} = 470 nm, λ_{em} = 520 nm) and the energy transfer in the spectrum was broad with more energy transfer from Zn_3N_2 to fluorescein. In this spectrum, the green color indicates the merging of emission spectrum of Zn_3N_2 and excitation spectrum of fluorescein and the yellow color indicates the DSBT. The broad spectrum of FRET channel also integrated with excitation of Zn_3N_2 and emission of fluorescein. This confirms that both the molecules are very close to each other with more energy efficiency toward the optical enhancement. In Figure 8c, the green color expressed the spectra overlap of the Zn_3N_2 emission spectrum with 535 nm excitation of neutral red. The energy transfer efficiency calculated[67] using the fluorescence intensity of the donor (Zn_3N_2) in the presence and absence of the acceptor (dyes) was found to be 91.9, 83.3, 96.1, and 98.2% for porphyrin@Zn_3N_2, FAD@Zn_3N_2, fluorescein@Zn_3N_2, and neutral red@Zn_3N_2, respectively. It also confirmed that FRET-dependent distance (i.e.) smaller than the intermolecular distance (neutral red@Zn_3N_2) induces more energy transfer (Figure 6d).

Influence of Zinc Nitride over Organic Dyes. With the confirmation of the FRET process, we explore the optical enhancement of organic dyes with the increase in the concentration of Zn_3N_2. The optical enhancement in fluorescence intensity of the organic dyes with the addition of Zn_3N_2 at various concentrations obtained using steady-state emission spectra and plotted in Figure 9. The visible enhancement in the intensity of the organic dyes such as porphyrin, FAD, fluorescein, and neutral red with the addition of Zn_3N_2 can be noted form the photographs obtained using the fiber optical probe given in the insets. Figure 9a shows the fluorescence emission spectra of porphyrin at 400 nm excitation. With an addition of Zn_3N_2 colloid from 0.3 to 4.5 μM, the fluorescence emission intensity at 625 nm has enhanced gradually with an increase in the concentration of Zn_3N_2 colloid. The increased fluorescence is considered as the significance of Zn_3N_2 and from the optical fiber-induced excitation photograph, prominent red emission is visibly

https://dx.doi.org/10.1021/acsami.9b21585
ACS Appl. Mater. Interfaces 2020, 12, 19245−19257

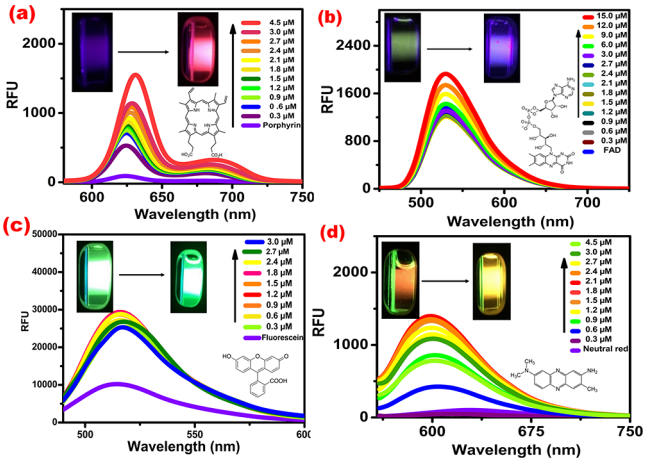

Figure 9. Fluorescence enhancement of dyes with the addition of Zn_3N_2, (a) porphyrin, (b) FAD (c) fluorescein, and (d) neutral red. Zn_3N_2 nanoparticles varied from a lower concentration of 0.3 μM to higher concentration of 4.5 μM.

observed (Figure 9a). The porphyrin dye in the absence of Zn_3N_2 relatively has very low intensity with the emission of feeble red colour. Nevertheless, with the addition of nanoparticles, the material turns into spectacular red emission with high intensity. The plot on Zn_3N_2 concentration versus the enhancement emission intensity is shown in Figure 10. For porphyrin, with the addition of lower concentration of 0.3 μM Zn_3N_2, the intensity is nearly 6 times higher than porphyrin alone. At a concentration of 4.5 μM of Zn_3N_2, the emission intensity of porphyrin enhances to the order of 20 times. The graph between fluorescence intensity and the concentration of Zn_3N_2 gives a good linear fitting within the limit of errors, and correlation coefficient was calculated as R^2 = 0.96514 (Figure 10a).

The fluorescence emission spectra of FAD with the addition of Zn_3N_2 colloid from 0.3 to 15 μM are given in Figure 9b. The FAD dye was excited at 445 nm, and we observed that the spectra with the green emission at 530 nm enhanced with the addition of Zn_3N_2. The influence of fluorescence intensity with the addition of Zn_3N_2 at a lower concentration of 0.3−1.8 μM is negligible. Nevertheless, after 2.1 μM, the fluorescence intensity enhances drastically with an increasing concentration of Zn_3N_2, and the emission intensity of FAD was enhanced to the order of 1.4 times. The prodigious enhancement in the green color emission could be observed from the photograph given in the inset of Figure 9b. The Zn_3N_2Vs intensity correlation graph shows good fit with the correlation coefficient of R^2 = 0.96786, as shown in Figure 10b.

For fluorescein@Zn_3N_2 (Figure 9c), the intensity increases from 0.3 to 1.8 μM Zn_3N_2 and gets saturated and then quenched in further addition of 2.1−3 μM. It shows that it reaches a threshold at 1.8 μM of Zn_3N_2 with an enhanced intensity to the order of 3.3 times. From the photographs of emission of the dyes, it could be easily visualized that with the addition of nanoparticles, the emission of green fluorescent spread up to top of the cuvette wall (Figure 9c). The nonlinear fitting of Zn_3N_2 concentration versus intensity has a good fit with a correlation coefficient of R^2 = 0.94597 (Figure 10c).

Figure 9d shows the emission spectral detail of the neutral red@Zn_3N_2 nanoparticle which increases from 0.3 to 1.5 μM, and the emission intensity enhanced to the order of 14 times and then started quenching on further addition of Zn_3N_2. The Zn_3N_2 concentration-dependent emission has nonlinear fitting with a correlation coefficient of R^2 = 0.98196 (Figure 10d). The photographs of all the emission of dyes clearly revealed that with an addition of Zn_3N_2, the emission intensifies, and it is totally concentration-dependent. In general, the fluorescence of the organic molecules related to the radiative transition from the first singlet state (S_1) to the ground singlet state (S_0). This kind of transition $S_1 \rightarrow S_0$ has a broad fluorescence emission with a longer life time.[68] Overall, the addition of Zn_3N_2 exhibits the broad spectrum of enhancement in emission with organic dyes, which can also be visualized without any optical tools. The binding energy graph (Figure S9) and the energy level diagram (Figure S10) shows FAD and fluorescein was not affected by the addition of Zn_3N_2. However, the shift in the emission wavelength of porphyrin and neutral red leads to the shift in the binding energy, which may be due to the functional group interactions with Zn_3N_2 nanoparticles.

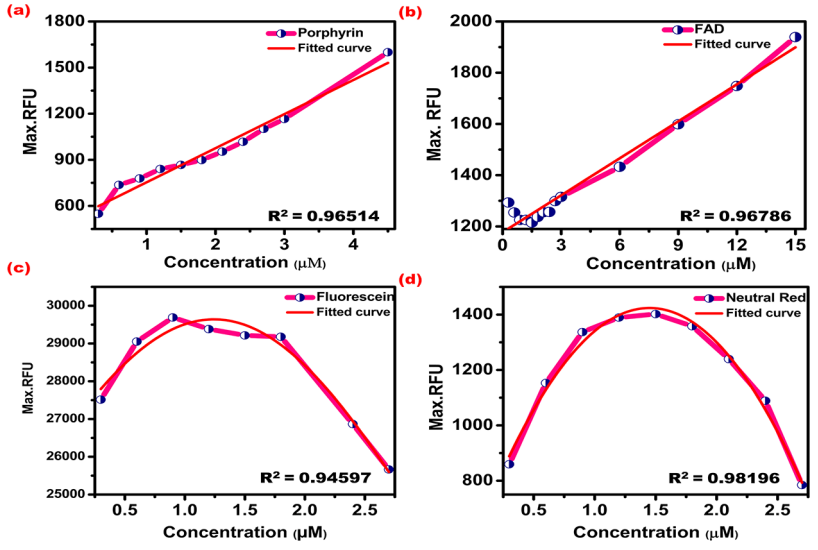

Figure 10. Fitted graph for concentration vs fluorescence intensity (a) porphyrin @Zn_3N_2, (b) FAD@Zn_3N_2, (c) fluorescein@Zn_3N_2, and (d) neutral red@Zn_3N_2.

https://dx.doi.org/10.1021/acsami.9b21585
ACS Appl. Mater. Interfaces 2020, 12, 19245−19257

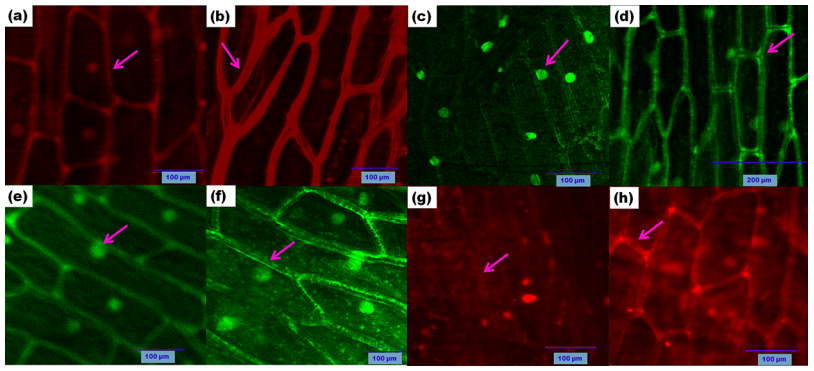

Figure 11. Confocal fluorescence image of plant cells (onion peel) with (a) porphyrin, (b) porphyrin@Zn_3N_2, (c) FAD, (d) FAD@Zn_3N_2, (e) fluorescein, (f) fluorescein@Zn_3N_2, (g) neutral red, and (h) neutral red@Zn_3N_2.

Live Cell Imaging. In order to prove the efficiency of Zn_3N_2 colloidal nanoparticle as an imaging probe, we have examined their implementation as fluorescent cell labels on plant cells (single layer onion peel) and animal cells (3T3 fibroblast cell) and imaged under a confocal laser scanning microscope. The inner monolayer of onion peels was loaded with both the chosen organic dyes and organic dyes@Zn_3N_2, and the influence of Zn_3N_2 was examined from the confocal fluorescence images.

Figure 11a shows the image of onion peels loaded with porphyrin alone, and it shows nucleus and the cell membrane tagged with the organic dye with low emission intensity. However, in the presence of porphyrin@Zn_3N_2 (Figure 11b) tagged with the cell membrane with enhanced intensity, where the thickness of the cell membranes and the intermediate gaps (indicated in arrow) and distance of separation from the adjacent cells is observed at high quality (Figure 11b). Similarly, for FAD dye alone (Figure 11c), the dye is majorly conjugated with nucleus, whereas with FAD@Zn_3N_2 (Figure 11d), it amplifies the visibility of the cell membrane. On comparing the images of fluorescein (Figure 11e) and fluorescein@Zn_3N_2 (Figure 11f), the enhancement is observed both on the cell membrane and to the nucleus, it also gives a beautiful 3D effect of the intermediate gaps of the adjacent cells by enhancing the fluorescence emission and also enhances the resolution. The plant cell effectively up takes neutral red (Figure 11g) and neutral red@Zn_3N_2 (Figure 11h). There is no distinguished visibility of cells in the presence of dye alone, whereas the cells are visible in the presence of neutral red@Zn_3N_2. The overlap of the bright-field image with the fluorescence image is shown in Figure S11. The intensity enhancement in cell organelles with the addition of Zn_3N_2 colloidal nanoparticles was quantified using ImageJ software and plotted in Figure S12. Porphyrin, FAD, fluorescein, and neutral red with the addition of Zn_3N_2 show around 75, 39, 66, and 65% of intensity enhancement, respectively.

The influence of fluorescence signals of organic dyes@Zn_3N_2 in the presence of animal cells was observed using 3T3 fibroblast cell lines, and the confocal images are shown in Figure 12. Prior to imaging, in order to confirm the cytotoxicity of dyes@Zn_3N_2, the MTT test was done at different concentrations (Figure S13). The results show very lesser cytotoxicity at lesser concentration of dye of about 0.3 μM, which is taken for cell culture imaging. Similar to the plant cells, there is also enhancement in the fluorescence signal of the cell membrane and nucleus. In the presence of porphyrin@Zn_3N_2 (Figure 12a), higher tagging is observed in the cell membrane, where cell microtubules are also observed to be tagged. The microtubule tagging is not observed in case of FAD@Zn_3N_2 (Figure 12b); however, the high quality nucleus structure is observed with higher resolution. The neutral red @Zn_3N_2 dye (Figure 12c) which shows comparatively lesser emission in plant cells shows good emission in human cells, where the nucleus and cell membrane are tagged and provide high-resolution imaging possibility. For fluorescein@Zn_3N_2 (Figure 12d), similar to plant cells, the dye is tagged both on the nucleus and the cell membrane.

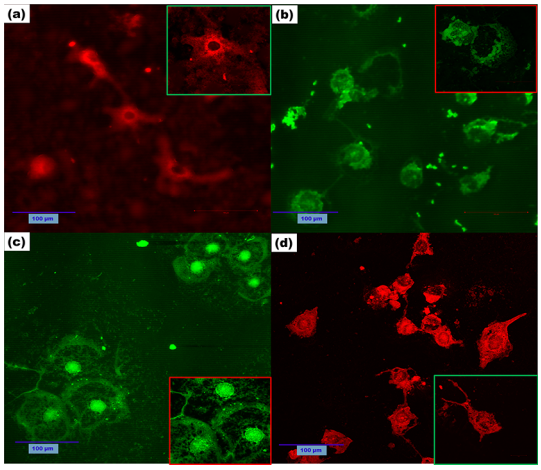

Figure 12. Confocal fluorescence image of 3T3 fibroblast cell with (a) porphyrin@Zn_3N_2, (b) FAD@Zn_3N_2, (c) fluorescein@Zn_3N_2, and (d) neutral red @Zn_3N_2.

The presence of Zn_3N_2 nanoparticles in 3T3 fibroblast is also witnessed by the SEM morphology assisted in situ mapping (Figure S14). It shows that in porphyrin@Zn_3N_2, FAD@Zn_3N_2, and fluorescein@Zn_3N_2, most of the zinc and nitrogen atoms were tagged on the cell membrane and nucleus of the cell. In the case of neutral red@Zn_3N_2, both nitrogen and zinc atoms were labeled on the cell membrane. These results are in good correlation with the confocal images of dye(s)@Zn_3N_2.

Discussion. The concept of fluorescence intensity enhancement is the salient feature in the field of biomedicine such as bioimaging and biosensors. Nonetheless, less toxic with enhanced fluorescence emission signals is a challenge due to the limitations in organic dyes such as stability, higher molecular weight, photobleaching, and so forth. To overcome this problem, researchers were trying to develop inorganic

https://dx.doi.org/10.1021/acsami.9b21585
ACS Appl. Mater. Interfaces 2020, 12, 19245−19257

nanoparticles with less toxicity. In this report, we have explored the combination of organic dyes with inorganic Zn_3N_2 colloidal nanoparticles, which can used as ultrabright fluorescent probes. The nanosized probe can serve as a sensitive biosensor for multiple analyte solution. Many of the nanoparticles have been approved by clinics such as iron oxide nanoparticles as contrast agents in MRI and gold nanoparticles as optical detectives on tumors and thermotherapy owing to its properties of hydrophilicity and stability.[69] Evidently, zinc nitride is considered as a nontoxic and earth-abundant element; so far it was not examined in the field of optical enhancements and its applications toward biomedical applications. Many other studies based on nanoparticles reported earlier for cell migration, growth, and differentiation were mostly based on organic dyes. However, this study focused on the fluorescence enhancement in the cell structure with respect to the addition of Zn_3N_2. In the present work, the synthesized Zn_3N_2 nanoparticles were successfully integrated with organic dyes such as protoporphyrin IX, FAD, fluorescein, and neutral red. The resulting material exhibits various enhanced properties, which can be used in biological application as a fluorescent label. Also, from the docking studies, we observed that the majority of the zinc molecules are attached with the dye molecules at a smaller intermolecular distance, which is the reason behind energy transfer (FRET) from Zn_3N_2 (donor) to organic dyes (acceptor). Hence, the addition of Zn_3N_2 colloid shows enhancement in the emission intensity up to 20 orders of organic dyes. The presence of Zn_3N_2 enhances the fluorescence signals of all the chosen dyes, and the molecular simulation studies show a good interaction with the organic dyes because of its hydrophobic nature. This also opens the possibility of interaction of larger drugs for therapy and diagnostic applications. Notably, in the present study, the enhancement of the fluorescent intensity is also observed with the naked eye and without the use of any optical tools opens the possibility of Zn_3N_2 for biosensor application. The cell uptake study in the presence of organic dye@Zn_3N_2 on both plant cells and animal cells showed a significant enhancement in emission signals, where the cell membrane, nucleus, and microtubules can be visualized at a higher resolution. This result revealed that this material has the potential for tagging the nuclear region with enhanced fluorescence of various cell lines, and with further studies, it can also be extended towards in vivo for diagnosis applications.

In the biomedical field, a variety of luminescent materials such as organic and inorganic nanoparticles, rare earth metal-doped upconversion nanoparticles and fluorescent proteins have been developed toward bioimaging applications. Organic nanoparticles and dyes are superior to other materials due to easy preparation and emission in the visible range. However, aggregation causes a quenching effect due to $\pi-\pi$ stacking. If it reacts with the bioenvironment, the hydrophobic nature of the dyes makes aggregates, and it will lead to self-quenching. Moreover, under high energy of excitation, photobleaching will be dominant compared to emission intensity.[70] However, in our present work, instead of photobleaching, the addition of zinc nitride colloidal in the dye medium makes enhanced emission intensity of the dye with longer stability. The quantum yield of the nanomaterials is affected by various factors including functionalization of the ligands on the surface of the material, solvent used for dispersion, and temperature of the reaction. Jiao et al.[71] synthesized silver indium sulfide quantum dots, using glutathione and polyethyleneimine and glutathione, behave as a ligand-based luminescence enhancement with the quantum yield of 37.2%. Lei et al.[72] work on zinc oxide/hyper branched poly ethylenimine nanocomposites (ZnO/HPEI) in different solvents gives a quantum yield of 30% in ethanol and 53% in chloroform and 11% in water, and (ZnO/HPEI) shows the blue fluorescence. However, in the present work, our Zn_3N_2 colloidal nanoparticle has a quantum efficiency of 59% without any further functionalization and any external solvent dispersion. In the past decade, a few works were reported in the zinc-related components such as ZnSe, ZnS,[73] and ZnSe@ZnSe[74] for bioimaging applications because of its wide bandgap and low toxicity. In the previous work of zinc nitride, nanocrystals reported only to study the size effect on the emission property of the nanocrystal from the visible to infrared region.[37] The room-temperature simple chemistry of synthesizing Zn_3N_2 colloidal nanoparticles and its potential toward biomedical applications are not yet reported. Herein, the smaller size of the zinc nitride colloidal nanoparticle induces the charge carrier confinement in bandgap discrimination of the energy states. This influences the FRET process and the photon mediated energy transfer in zinc nitride (donor) prompt the radiative energy transfer to dyes-(acceptor), which is depicted in Figure 8. Therefore, the efficiency of the zinc nitride has a good ability to absorb and emit photons with a high quantum yield. Figure 8 shows the overlap of spectrum data, from that the energy resonance process between the donor and acceptor drives more energy transfer even upto 98% (i.e. neutral red@Zn_3N_2). This study also demonstrates the successful elimination of photobleaching of dyes through the FRET process through integrated with Zn_3N_2 colloidal nanoparticles, which can be potentially used in cellular imaging.

CONCLUSIONS

In summary, we have successfully prepared Zn_3N_2 colloidal nanoparticles at room temperature using the chemical method and investigated their fluorescence enhancement toward bioimaging application. This is the first report to express the possibility of zinc nitride for biomedical applications. The average particle size is observed to be around 25 nm, and the fluorescence emission is at 415 nm (blue emission). The fluorescence sensitive of Zn_3N_2 over organic dyes is evidenced from the enhanced emission intensity of dyes such as porphyrin, FAD, fluorescein, and neutral red in presence of the nanoparticle. The optical emission enhancement of the organic dye(s) may be due to the FRET between the Zn_3N_2 nanoparticles and organic dyes, evidenced from molecular docking studies and lifetime measurements. When Zn_3N_2 colloid and organic dyes are used as fluorescence labels for confocal imaging of plant cells and animal cells, enhanced emission signal is observed with good qualitative images. We conclude that Zn_3N_2 colloidal nanoparticles in future have a great potential for biosensor and bioimaging applications.

ASSOCIATED CONTENT

Supporting Information

The Supporting Information is available free of charge at https://pubs.acs.org/doi/10.1021/acsami.9b21585.

XRD pattern of the zinc nitride nanoparticle; TEM image at different magnifications; EDAX spectrum; validation of emission of Zn_3N_2 due to zinc nitride; variation of fluorescence intensity as a function of days

https://dx.doi.org/10.1021/acsami.9b21585
ACS Appl. Mater. Interfaces 2020, 12, 19245−19257

for observing the stability of Zn_3N_2 colloids; UV−vis spectrum of dyes against various concentrations of Zn_3N_2: porphyrin Zn_3N_2, FAD@Zn_3N_2, fluorescein@Zn_3N_2, and neutral red@Zn_3N_2; scheme for Jablonski energy level diagram for organic dyes and FRET energy transfer from Zn_3N_2 nanoparticles to organic dyes; dyes@Zn_3N_2 excited by 340 nm to confirm the presence of Zn_3N_2 in dyes@Zn_3N_2; binding energy of dyes and dyes@Zn_3N_2; energy level diagram for dyes and dyes@Zn_3N_2; the overlap of bright-field image with the fluorescence image, after the addition of Zn_3N_2 nanoparticles to organic dyes; quantification of the intensity before and after the addition of zinc nitride to the dyes treated in the cells calculated from ImageJ software; cytotoxicity of the Zn_3N_2 nanoparticle with various concentrations from 0.3 to 1.5 μM; and SEM mapping for cells tagged with nanoparticles: porphyrin@Zn_3N_2, FAD@Zn_3N_2, fluorescein@Zn_3N_2, and neutral red@Zn_3N_2 (PDF)

AUTHOR INFORMATION

Corresponding Author

Dhinasekaran Durgalakshmi − *Department of Medical Physics, Anna University, Chennai 600025, India;* orcid.org/0000-0002-1281-6539; Email: durgaklakshmi@gmail.com

Authors

Soundharraj Prabha − *Department of Medical Physics, Anna University, Chennai 600025, India*

Karthikeyan Subramani − *Department of Organic Chemistry, Science Faculty, Peoples' Friendship University of Russia (RUDN University), Moscow 117198, Russia*

Prakasarao Aruna − *Department of Medical Physics, Anna University, Chennai 600025, India*

Singaravelu Ganesan − *Department of Medical Physics, Anna University, Chennai 600025, India*

Complete contact information is available at: https://pubs.acs.org/10.1021/acsami.9b21585

Notes

The authors declare no competing financial interest.

ACKNOWLEDGMENTS

One of the authors D.D. gratefully acknowledges DST-INSPIRE Faculty Fellowship under the sanction DST/INSPIRE/04/2016/000845 for their funding. The authors also acknowledge project of UGC-UPE [10466/PD1/UPE/2016] for confocal microscopy facility and DST-FST[SR/FST/PS1-214/2016(c)] for Aqualog instrument.

REFERENCES

(1) Mei, J.; Huang, Y.; Tian, H. Progress and Trends in AIE-Based Bioprobes: A Brief Overview. *ACS Appl. Mater. Interfaces* **2017**, *10*, 12217−12261.

(2) Xu, J.; Gulzar, A.; Yang, P.; Bi, H.; Yang, D.; Gai, S.; He, F.; Lin, J.; Xing, B.; Jin, D. Recent Advances in Near-Infrared Emitting Lanthanide-Doped Nanoconstructs: Mechanism, Design and Application for Bioimaging. *Coord. Chem. Rev.* **2019**, *381*, 104−134.

(3) Bhattacharyya, K.; Mukherjee, S. Fluorescent Metal Nano-Clusters as Next Generation Fluorescent Probes for Cell Imaging and Drug Delivery. *Bull. Chem. Soc. Jpn.* **2018**, *91*, 447−454.

(4) Wolfbeis, O. S. An Overview of Nanoparticles Commonly Used in Fluorescent Bioimaging. *Chem. Soc. Rev.* **2015**, *44*, 4743−4768.

(5) Michalet, X.; Pinaud, F. F.; Bentolila, L. A.; Tsay, J. M.; Doose, S.; Li, J. J.; Sundaresan, G.; Wu, A.; Gambhir, S.; Weiss, S. Quantum Dots for Live Cells, in Vivo Imaging, and Diagnostics. *Science* **2005**, *307*, 538−544.

(6) Ozawa, T.; Yoshimura, H.; Kim, S. B. Advances in Fluorescence and Bioluminescence Imaging. *Anal. Chem.* **2012**, *85*, 590−609.

(7) Shi, J.; Tian, F.; Lyu, J.; Yang, M. Nanoparticle Based Fluorescence Resonance Energy Transfer (FRET) for Biosensing Applications. *J. Mater. Chem. B* **2015**, *3*, 6989−7005.

(8) Charron, D. M.; Zheng, G. Nanomedicine Development Guided by FRET Imaging. *Nano Today* **2018**, *18*, 124−136.

(9) Lumdee, C.; Yun, B.; Kik, P. G. Gap-Plasmon Enhanced Gold Nanoparticle Photoluminescence. *ACS Photonics* **2014**, *1*, 1224−1230.

(10) Wang, J.; Moore, J.; Laulhe, S.; Nantz, M.; Achilefu, S.; Kang, K. A. Fluorophore−Gold Nanoparticle Complex for Sensitive Optical Biosensing and Imaging. *Nanotechnology* **2012**, *23*, 095501.

(11) Resch-Genger, U.; Grabolle, M.; Cavaliere-Jaricot, S.; Nitschke, R.; Nann, T. Quantum Dots Versus Organic Dyes as Fluorescent Labels. *Nat. Methods* **2008**, *5*, 763.

(12) Liang, R.; Wei, M.; Evans, D. G.; Duan, X. Inorganic Nanomaterials for Bioimaging, Targeted Drug Delivery and Therapeutics. *Chem. Commun.* **2014**, *50*, 14071−14081.

(13) Ballou, B.; Ernst, L.; Waggoner, A. Fluorescence Imaging of Tumors in Vivo. *Curr. Med. Chem.* **2005**, *12*, 795−805.

(14) Wang, Y.; Chen, J.-T.; Yan, X.-P. Fabrication of Transferrin Functionalized Gold Nanoclusters/Graphene Oxide Nanocomposite for Turn-on Near-Infrared Fluorescent Bioimaging of Cancer Cells and Small Animals. *Anal. Chem.* **2013**, *85*, 2529−2535.

(15) Eixenberger, J. E.; Anders, C. B.; Wada, K.; Reddy, K. M.; Brown, R. J.; Moreno-Ramirez, J.; Weltner, A. E.; Karthik, C.; Tenne, D. A.; Fologea, D.; Wingett, D. G. Defect Engineering of Zno Nanoparticles for Bio-Imaging Applications. *ACS Appl. Mater. Interfaces* **2019**, *11*, 24933−24944.

(16) Huo, F.; Liu, Y.; Zhu, M.; Gao, E.; Zhao, B.; Yang, X. Ultrabright Full Color Carbon Dots by Fine-Tuning Crystal Morphology Controllable Synthesis for Multicolor Bioimaging and Sensing. *ACS Appl. Mater. Interfaces* **2019**, *11*, 27259−27268.

(17) Dineshkumar, S.; Raj, A.; Srivastava, A.; Mukherjee, S.; Pasha, S. S.; Kachwal, V.; Fageria, L.; Chowdhury, R.; Laskar, I. R. Facile Incorporation of "Aggregation-Induced Emission"-Active Conjugated Polymer into Mesoporous Silica Hollow Nanospheres: Synthesis, Characterization, Photophysical Studies, and Application in Bioimaging. *ACS Appl. Mater. Interfaces* **2019**, *11*, 31270−31282.

(18) Kesarwani, V.; Kelly, H. G.; Shankar, M.; Robinson, K. J.; Kent, S. J.; Traven, A.; Corrie, S. R. Characterization of Key Bio−Nano Interactions Between Organosilica Nanoparticles and Candida Albicans. *ACS Appl. Mater. Interfaces* **2019**, *11*, 34676−34687.

(19) Zhang, Y.; Bai, Y.; Jia, J.; Gao, N.; Li, Y.; Zhang, R.; Jiang, G.; Yan, B. Perturbation of Physiological Systems by Nanoparticles. *Chem. Soc. Rev.* **2014**, *43*, 3762−3809.

(20) Pellegrini, G.; Mattei, G.; Mazzoldi, P. Finite Depth Square Well Model: Applicability and Limitations. *J. Appl. Phys.* **2005**, *97*, 073706.

(21) Anikeeva, P. O.; Halpert, J. E.; Bawendi, M. G.; Bulović, V. Quantum Dot Light-Emitting Devices with Electroluminescence Tunable Over the Entire Visible Spectrum. *Nano Lett.* **2009**, *9*, 2532−2536.

(22) Fernée, M. J.; Jensen, P.; Rubinsztein-Dunlop, H. Origin of the Large Homogeneous Line Widths Obtained from Strongly Quantum Confined Pbs Nanocrystals at Room Temperature. *J. Phys. Chem. C* **2007**, *111*, 4984−4989.

(23) Ma, W.; Swisher, S. L.; Ewers, T.; Engel, J.; Ferry, V. E.; Atwater, H. A.; Alivisatos, A. P. Photovoltaic Performance of Ultrasmall Pbse Quantum Dots. *ACS Nano* **2011**, *5*, 8140−8147.

(24) Keuleyan, S.; Lhuillier, E.; Guyot-Sionnest, P. Synthesis of Colloidal Hgte Quantum Dots for Narrow Mid-IR Emission and Detection. *J. Am. Chem. Soc.* **2011**, *133*, 16422−16424.

(25) Grim, J. Q.; Manna, L.; Moreels, I. A Sustainable Future for Photonic Colloidal Nanocrystals. *Chem. Soc. Rev.* **2015**, *44*, 5897−5914.
(26) Prasad, A. S. Zinc is an Antioxidant and Anti-Inflammatory Agent: Its Role in Human Health. *Front. Nutr.* **2014**, *1*, 14.
(27) Chasapis, C. T.; Loutsidou, A. C.; Spiliopoulou, C. A.; Stefanidou, M. E. Zinc and Human Health: An Update. *Arch. Toxicol.* **2012**, *86*, 521−534.
(28) Roohani, N.; Hurrell, R.; Kelishadi, R.; Schulin, R. Zinc and its Importance for Human Health: An Integrative Review. *J. Res. Med. Sci.* **2013**, *18*, 144−157.
(29) Premkumar, T.; Vidya, R. Crystal and Electronic Structure Studies on Transparent Conducting Nitrides A3N2 (A= Mg, Zn and Sn) and Sn3N4. *Mater. Res. Express* **2019**, *6*, 055912.
(30) Kuriyama, K.; Takahashi, Y.; Sunohara, F. Optical Band Gap of Zn3N2 Films. *Phys. Rev. B: Condens. Matter Mater. Phys.* **1993**, *48*, 2781.
(31) Chinnakutti, K. K.; Thanharaj Salammal, S.; Panneerselvam, V.; Parasuraman, K.; Vishwakarma, V. Highly Transparent Zinc Nitride Thin Films by RF Magnetron Sputtering with Enhanced Optoelectronic Behavior. *Mater. Sci. Eng. B* **2018**, *232*−*235*, 33−40.
(32) Zong, F.; Ma, H.; Ma, J.; Du, W.; Zhang, X.; Xiao, H.; Ji, F.; Xue, C. Structural Properties and Photoluminescence of Zinc Nitride Nanowires. *Appl. Phys. Lett.* **2005**, *87*, 233104.
(33) Yang, T.; Zhang, Z.; Li, Y.; Lv, M.; Song, S.; Wu, Z.; Yan, J.; Han, S. Structural and Optical Properties of Zinc Nitride Films Prepared by Rf Magnetron Sputtering. *Appl. Surf. Sci.* **2009**, *255*, 3544−3547.
(34) Futsuhara, M.; Yoshioka, K.; Takai, O. Optical Properties of Zinc Oxynitride Thin Films. *Thin Solid Films* **1998**, *317*, 322−325.
(35) Da Cunha, P. R. C. R. Deposition of Znxny Thin Films and Application in TFT Structures. M.Sc Thesis, Técnico Lisboa, 2013.
(36) Ahumada-Lazo, R.; Fairclough, S. M.; Hardman, S. J. O.; Taylor, P. N.; Green, M.; Haigh, S. J.; Saran, R.; Curry, R. J.; Binks, D. J. Confinement Effects and Charge Dynamics in Zn3N2 Colloidal Quantum Dots: Implications for QD-LED Displays. *ACS Appl. Nano Mater.* **2019**, *2*, 7214−7219.
(37) Taylor, P. N.; Schreuder, M. A.; Smeeton, T. M.; Grundy, A. J. D.; Dimmock, J. A. R.; Hooper, S. E.; Heffernan, J.; Kauer, M. Synthesis of Widely Tunable and Highly Luminescent Zinc Nitride Nanocrystals. *J. Mater. Chem. C* **2014**, *2*, 4379−4382.
(38) Lang, P. T.; Brozell, S. R.; Mukherjee, S.; Pettersen, E. F.; Meng, E. C.; Thomas, V.; Rizzo, R. C.; Case, D. A.; James, T. L.; Kuntz, I. D. DOCK 6: Combining Techniques to Model RNA−Small Molecule Complexes. *RNA* **2009**, *15*, 1219−1230.
(39) Moustakas, D. T.; Lang, P. T.; Pegg, S.; Pettersen, E.; Kuntz, I. D.; Brooijmans, N.; Rizzo, R. C. Development and Validation of a Modular, Extensible Docking Program: DOCK 5. *J. Comput.-Aided Mol. Des.* **2006**, *20*, 601−619.
(40) Morris, G. M.; Huey, R.; Lindstrom, W.; Sanner, M. F.; Belew, R. K.; Goodsell, D. S.; Olson, A. J. Autodock4 and Autodocktools4: Automated Docking with Selective Receptor Flexibility. *J. Comput. Chem.* **2009**, *30*, 2785−2791.
(41) Morris, G. M.; Goodsell, D. S.; Halliday, R. S.; Huey, R.; Hart, W. E.; Belew, R. K.; Olson, A. J. Automated Docking using a Lamarckian Genetic Algorithm and an Empirical Binding Free Energy Function. *J. Comput. Chem.* **1998**, *19*, 1639−1662.
(42) Huey, R.; Morris, G. M.; Olson, A. J.; Goodsell, D. S. A Semiempirical Free Energy Force Field with Charge-Based Desolvation. *J. Comput. Chem.* **2007**, *28*, 1145−1152.
(43) Lavand, A. B.; Malghe, Y. S. Synthesis, Characterization and Visible Light Photocatalytic Activity of Nitrogen-Doped Zinc Oxide Nanospheres. *J. Asian Ceram. Soc.* **2015**, *3*, 305−310.
(44) Lin, C.-W.; Song, Y.-P.; Chang, S.-C. Rapid Thermal Oxidation of Zinc Nitride Film. *Jpn. J. Appl. Phys.* **2015**, *54*, 04DH06.
(45) Zhang, Z.-X.; Pan, X.-J.; Liu, L.-X.; Ma, Z.-W.; Zhao, H.-T.; Jia, L.; Xie, E.-Q. Green Photoluminescence from Zn3N2: Tb Films Prepared by Magnetron Sputtering. *J. Appl. Phys.* **2009**, *105*, 016101.
(46) Manjón, F. J.; Marí, B.; Serrano, J.; Romero, A. H. Silent Raman Modes in Zinc Oxide and Related Nitrides. *J. Appl. Phys.* **2005**, *97*, 053516.
(47) Kaschner, A.; Haboeck, U.; Strassburg, M.; Strassburg, M.; Kaczmarczyk, G.; Hoffmann, A.; Thomsen, C.; Zeuner, A.; Alves, H. R.; Hofmann, D. M.; Meyer, B. K. Nitrogen-Related Local Vibrational Modes in Zno: N. *Appl. Phys. Lett.* **2002**, *80*, 1909−1911.
(48) Alimohammadi, H. Effect of Oxidation on the Optical Properties of Zn3N2 Powders, Ph.D Dissertation, University of Victoria, 2017.
(49) Cao, X.; Sato, A.; Ninomiya, Y.; Yamada, N. Oxygen-Doped Zinc Nitride as a High-Mobility Nitride-Based Semiconductor. *J. Phys. Chem. C* **2015**, *119*, 5327−5333.
(50) Perumal, R.; Casale, S.; De Stefano, L.; Spadavecchia, J. Synthesis and Characterization of Ag-Protoporphyrin Nano Structures using Mixed Co-Polymer Method. *Front. Lab. Med.* **2017**, *1*, 49−54.
(51) Bera, K.; Maiti, S.; Maity, M.; Mandal, C.; Maiti, N. C. Porphyrin−Gold Nanomaterial for Efficient Drug Delivery to Cancerous Cells. *ACS Omega* **2018**, *3*, 4602−4619.
(52) Ashjari, M.; Dehfuly, S.; Fatehi, D.; Shabani, R.; Koruji, M. Efficient Functionalization of Gold Nanoparticles using Cysteine Conjugated Protoporphyrin IX for Singlet Oxygen Production in Vitro. *RSC Adv.* **2015**, *5*, 104621−104628.
(53) Chithra, K.; Aruna, P.; Einstein, G.; Vijayaraghavan, S.; Ganesan, S. Monitoring Breast Cancer Response to Treatment using Stokes Shift Spectroscopy of Blood Plasma. *J. Fluoresc.* **2019**, *29*, 803−812.
(54) Bubniene, U.; Mazetyte, R.; Ramanaviciene, A.; Gulbinas, V.; Ramanavicius, A.; Karpicz, R. Fluorescence Quenching-Based Evaluation of Glucose Oxidase Composite with Conducting Polymer, Polypyrrole. *J. Phys. Chem. C* **2018**, *122*, 9491−9498.
(55) Sivabalan, S.; Vedeswari, C. P.; Jayachandran, S.; Koteeswaran, D.; Pravda, C.; Aruna, P. R.; Ganesan, S. In Vivo Native Fluorescence Spectroscopy and Nicotinamide Adinine Dinucleotide/Flavin Adenine Dinucleotide Reduction and Oxidation States of Oral Submucous Fibrosis for Chemopreventive Drug Monitoring. *J. Biomed. Optic.* **2010**, *15*, 017010.
(56) Prakash, A.; Pathrose, B. P.; Mathew, S.; Nampoori, V. P. N.; Radhakrishnan, P.; Mujeeb, A. Variations in Thermo-Optical Properties of Neutral Red Dye with Laser Ablated Gold Nanoparticles. *Opt. Mater.* **2018**, *79*, 237−242.
(57) Prabha, S.; Durgalakshmi, D.; Aruna, P.; Ganesan, S. Influence of the Parameters in the Preparation of Silica Nanoparticles from Biomass and Chemical Silica Precursors Towards Bioimaging Application. *Vacuum* **2019**, *160*, 181−188.
(58) Chinnathambi, S.; Velmurugan, D.; Hanagata, N.; Aruna, P. R.; Ganesan, S. Investigations on the Interactions of 5-Fluorouracil with Bovine Serum Albumin: Optical Spectroscopic and Molecular Modeling Studies. *J. Lumin.* **2014**, *151*, 1−10.
(59) Wang, M.; Tang, F.; Pan, X.; Yao, L.; Wang, X.; Jing, Y.; Ma, J.; Wang, G.; Mi, L. Rapid Diagnosis and Intraoperative Margin Assessment of Human Lung Cancer with Fluorescence Lifetime Imaging Microscopy. *BBA Clin.* **2017**, *8*, 7−13.
(60) Chou, K.; Dennis, A. Förster Resonance Energy Transfer between Quantum Dot Donors and Quantum Dot Acceptors. *Sensors* **2015**, *15*, 13288−13325.
(61) Kang, H.; Clarke, M. L.; Lacerda, S. H. D. P.; Karim, A.; Pease, L. F.; Hwang, J. Multimodal Optical Studies of Single and Clustered Colloidal Quantum Dots for the Long-Term Optical Property Evaluation of Quantum Dot-Based Molecular Imaging Phantoms. *Biomed. Optic Express* **2012**, *3*, 1312−1325.
(62) Shi, J.; Chan, C.; Pang, Y.; Ye, W.; Tian, F.; Lyu, J.; Zhang, Y.; Yang, M. A Fluorescence Resonance Energy Transfer (FRET) Biosensor based on Graphene Quantum Dots (Gqds) and Gold Nanoparticles (Aunps) for the Detection of Meca Gene Sequence of Staphylococcus Aureus. *Biosens. Bioelectron.* **2015**, *67*, 595−600.

https://dx.doi.org/10.1021/acsami.9b21585
ACS Appl. Mater. Interfaces 2020, 12, 19245−19257

(63) Reis, A. F.; Monte, A. F. G.; Alves, G. A. Evidence of Resonant Energy Transfer between Cdse/Zns Quantum Dots and Neutral Red Dye Molecules. *J. Lumin.* **2018**, *204*, 349−353.
(64) Lai, T.-H.; Constantinou, I.; Grand, C. M.; Klump, E. D.; Baek, S.; Hsu, H.-Y.; Tsang, S.-W.; Schanze, K. S.; Reynolds, J. R.; So, F. Evidence of Molecular Structure Dependent Charge Transfer between Isoindigo-Based Polymers and Fullerene. *Chem. Mater.* **2016**, *28*, 2433−2440.
(65) Chen, Y.; Mauldin, J. P.; Day, R. N.; Periasamy, A. Characterization of Spectral FRET Imaging Microscopy for Monitoring Nuclear Protein Interactions. *J. Microsc.* **2007**, *228*, 139−152.
(66) Mcgrath, N.; Barroso, M. Quantum Dots as Fluorescence Resonance Energy Transfer Donors in Cells. *J. Biomed. Optic.* **2008**, *13*, 031210.
(67) Devatha, G.; Rao, A.; Roy, S.; Pillai, P. P. FöRster Resonance Energy Transfer Regulated Multicolor Photopatterning from Single Quantum Dot Nanohybrid Films. *ACS Energy Lett.* **2019**, *4*, 1710−1716.
(68) Berezin, M. Y.; Achilefu, S. Fluorescence Lifetime Measurements and Biological Imaging. *Chem. Rev.* **2010**, *110*, 2641−2684.
(69) Singh, P.; Pandit, S.; Mokkapati, V. R. S. S.; Garg, A.; Ravikumar, V.; Mijakovic, I. Gold Nanoparticles in Diagnostics and Therapeutics for Human Cancer. *Int. J. Mol. Sci.* **2018**, *19*, 1979.
(70) Chen, S.; Wang, H.; Hong, Y.; Tang, B. Z. Fabrication of Fluorescent Nanoparticles based on AIE Luminogens (AIE Dots) and their Applications in Bioimaging. *Mater. Horiz.* **2016**, *3*, 283−293.
(71) Jiao, M.; Li, Y.; Jia, Y.; Li, C.; Bian, H.; Gao, L.; Cai, P.; Luo, X. Strongly Emitting and Long-Lived Silver Indium Sulfide Quantum Dots for Bioimaging: Insight into Co-Ligand Effect on Enhanced Photoluminescence. *J. Colloid Interface Sci.* **2020**, *565*, 35−42.
(72) Lei, G.; Yang, S.; Cao, R.; Zhou, P.; Peng, H.; Peng, R.; Zhang, X.; Yang, Y.; Li, Y.; Wang, M.; He, Y.; Zhou, L.; Du, J.; Du, W.; Shi, Y.; Wu, H. In Situ Preparation of Amphibious Zno Quantum Dots with Blue Fluorescence Based on Hyperbranched Polymers and their Application in Bio-Imaging. *Polymers* **2020**, *12*, 144.
(73) Caires, A. J.; Mansur, A. A. P.; Carvalho, I. C.; Carvalho, S. M.; Mansur, H. S. Green Synthesis of Zns Quantum Dot/Biopolymer Photoluminescent Nanoprobes for Bioimaging Brain Cancer Cells. *Mater. Chem. Phys.* **2020**, *244*, 122716.
(74) Li, C.; Wu, P. Cu-Doped Quantum Dots: A New Class of Near-Infrared Emitting Fluorophores for Bioanalysis and Bioimaging. *Luminescence* **2019**, *34*, 782−789.

https://dx.doi.org/10.1021/acsami.9b21585
ACS Appl. Mater. Interfaces 2020, 12, 19245−19257